Applied Clay Science 210 (2021) 106124

Contents lists available at ScienceDirect

Applied Clay Science

journal homepage: www.elsevier.com/locate/clay

Closing repository void spaces using bentonite: does heat make a difference?

K.A. Daniels [a,*], J.F. Harrington [a], P. Sellin [b], S. Norris [c]

[a] British Geological Survey, Nicker Hill, Keyworth, Nottinghamshire, NG12 5GG, UK
[b] Svensk Karnbranslehantering AB (SKB), Brahegatan 47, Stockholm 10240, Sweden
[c] Radioactive Waste Management Limited (RWM), Thomson Avenue, Harwell Campus, Didcot, Oxfordshire, OX11 0GD, UK

ARTICLE INFO

Keywords:
Radioactive waste disposal engineered barrier system bentonite homogenisation elevated temperature swelling pressure

ABSTRACT

Bentonites are commonly proposed for use in the geological disposal of high heat generating radioactive wastes. Repository designs include bentonite as a buffer to occupy the void space around the waste canisters because of the favourable properties it can exhibit that enhance the isolation and containment functionality of the repository. Many repository concepts introduce small voids within the bentonite because the buffer is incorporated as individual bricks stacked around the waste canisters. These voids must be closed to prevent the persistence of high permeability pathways for fluids. As bentonite hydrates, it expands and can exert a considerable swelling pressure on the surrounding host rock. The bentonite also expands to fill the engineering cavities inherently present in the repository, but the non-uniform development of total stress and pore pressure could cause persistent material heterogeneities to occur. This is likely to be exacerbated by the thermal gradients existing between the hot waste and the temperature of the surrounding host rock in the early stages of repository post-closure. Whilst this is an area of ongoing research, the final extent of bentonite homogenisation within the repository and for how long property variations persist, is not well understood.

In this study, four tests were conducted on pre-compacted, sodium-activated MX80 bentonite samples placed next to a water-filled engineering void, to examine the effect of elevated temperature on the development of swelling and swelling pressure as a function of sample size. The sample lengths were chosen to give small bentonite-to-void ratios, and to represent extremities of behaviour, such that an acceptable upper limit of void size might be established. The results demonstrated that even under extreme bentonite-to-void ratios, the bentonite was able to swell and completely fill the void space, exerting a small but measurable swelling pressure. Under the conditions of this study, the results have shown larger end-of-test swelling pressures and higher final dry densities along their entire length than shown in equivalent tests conducted at ambient temperature. In addition, the elevated temperature tests showed a rapid initial increase and then decrease in swelling pressure at the start of testing, approaching an asymptote in swelling pressure more quickly, whilst uptaking less water than in the ambient temperature case. This implied that heating the bentonite reduced the test duration by about 60%, which is most likely explained by a reduction in the viscosity of the test permeant at higher temperatures.

1. Introduction

Radioactive waste is generated as a by-product of the production of energy from nuclear fuels, and consequently the safe and long-term disposal of this waste is an inevitable requirement. In the UK, the Nuclear Decommissioning Authority is responsible for clearing up 17 nuclear legacy sites from the post-war era (NDA, 2016), and thus safely disposing of High (HLW), Intermediate (ILW) and Low Level (LLW) Wastes in a repository will need to take place. Repository designs universally favour geological disposal of HLW and ILW. The high heat generating wastes (HHGW) (e.g. HLW and spent fuels (SF)) will be placed in a canister with a clay buffer material occupying the void space around the waste (Sellin and Leupin, 2013). Low heat generating wastes (LHGW) (e.g. ILW and LLW) on the other hand will be disposed of in a separate part of the geological disposal facility (GDF) and likely be surrounded by a cementitious backfill. The type of geology available for the construction of a repository at the correct depth below the ground surface will dictate exactly how the GDF is to be designed and the

* Corresponding author.
E-mail address: katdan@bgs.ac.uk (K.A. Daniels).

https://doi.org/10.1016/j.clay.2021.106124
Received 6 November 2020; Received in revised form 28 April 2021; Accepted 3 May 2021
Available online 31 May 2021

barriers to be used (Chapman, 2006; Delage et al., 2010; Chapman and Hooper, 2012; Sellin and Leupin, 2013). The buffer around the waste forms part of the engineered barrier system (EBS), and this must be able to contain contaminated fluids and prevent their migration from the disposal site into the surrounding environment (Komine, 2010; Svoboda, 2013). For HHGWs, this means that the buffer should have a very low permeability whilst being able to withstand the high temperatures produced by decaying radioactive waste without degrading. Degradation of the EBS could occur mechanically and/or chemically and would likely lead to an increased permeability, reducing its sealing performance (Nakayama et al., 2004; Karnland et al., 2007; Cuisinier et al., 2008; Herbert et al., 2008; Fernández et al., 2009; Ye et al., 2014).

Bentonite is commonly proposed for use as the buffer material in the EBS in many proposed HHGW facilities (Pusch, 2002; Wersin et al., 2007; Gens et al., 2013) because of its very low permeability, high swelling capacity and self-sealing characteristics (Deniau et al., 2008; Villar and Lloret, 2008; Zheng et al., 2015; Daniels et al., 2017). An accurate knowledge of its long-term behaviour under a range of appropriate thermo-hydro-mechanical-chemical (THMC) conditions is thus required before it can be confidently used in the repository scenario, where an adequate performance over long time periods is needed (NEA-OECD, 2004). The effect of temperature on the hydraulic properties of bentonite has been an active research area for some decades (Karnland et al., 1994; Börgesson et al., 1995; Börgesson and Hernelind, 1999; Cho et al., 1999; Romero et al., 2001; Rutqvist et al., 2001; Villar and Lloret, 2004; Ye et al., 2013, 2014; Harrington et al., 2014; Daniels et al., 2017), and more recently the effect of temperature on the swelling properties has also been receiving attention (Karnland et al., 1994; Tang and Cui, 2005; Tang et al., 2008; Tang and Cui, 2009; Ye et al., 2013, 2014). In addition, as many repository concepts incorporate the EBS as bricks stacked around the waste canisters (Andra, 2005; Martin et al., 2006; Juvankoski, 2010; Wang et al., 2013), small cavities or engineering voids between the bricks are intially introduced (Gatabin et al., 2016; Jia et al., 2019). The choice of material must be able to achieve adequate performance standards in terms of the overall dry density Jia et al. (2019) and demonstrate that these engineering voids would not be a high permeability pathway for fluids.

Previous studies have investigated the role of engineering voids on the hydromechanical behaviour of bentonite-based materials (Gens et al., 2011; Wang et al., 2013; Mokni et al., 2016; Bian et al., 2018; Harrington et al., 2020; Zeng et al., 2020; Watanabe and Yokoyama, 2021). As a smectite rich material, bentonite is able to expand into these engineering voids to isolate heat-emitting waste (Villar and Lloret, 2008; Wang et al., 2013; Bian et al., 2018; Harrington et al., 2020; Zeng et al., 2020; Watanabe and Yokoyama, 2021). However, the rate at which this process occurs will be dependent on a number of factors including the waste temperature, the magnitude of the pore-pressure and fluid availability. The swelling may also affect the hydro-mechanical properties as it correlates with a decrease in the dry density (Komine et al., 2009; Komine, 2010; Dueck et al., 2016; Bian et al., 2018; Dueck et al., 2019; Harrington et al., 2020). Consequently, non-uniform swelling pressure development may result in material heterogeneity in terms of density, permeability and mechanical property variations (Bian et al., 2018; Harrington et al., 2020; Zeng et al., 2020) because some parts of the material have expanded more than others; this could affect the bentonite performance as a mechanical and flow barrier. Bentonite homogenisation and material heterogeneity are thus important topics and are beginning to receive additional attention (Dueck et al., 2011, 2014, 2016, 2018, 2019; Harrington et al., 2020; Sellin et al., 2020).

To gain a further understanding of the extent of material heterogeneity, laboratory experiments examining the capacity of pre-compacted bentonite to swell into a void at elevated temperature have been performed. In these tests, a sample of pre-compacted MX80 bentonite installed in a constant volume apparatus with a fluid-filled void above, and subjected to in-situ repository conditions, was allowed to swell into the void space whilst the swelling pressures around the sample were continuously monitored. The tests were conducted at an elevated temperature and different starting lengths of sample were tested. The tests were designed to recreate a worst-case scenario to examine whether, with a large material-to-void ratio, a bentonite barrier could swell and achieve void filling. In addition, the tests presented here do not examine the role of the thermal gradient, but are applicable at the outer edges of the barrier, or where high thermal conductivity bentonites are used to minimise the thermal gradient (Rutqvist, 2020). At the outer edges of the barrier furthest from the waste canisters, the thermal gradient is likely to be small (Zhang et al., 2007, 2009, 2017) but groundwater will be more readily available. The results of these tests have then been compared with the results of three tests conducted at ambient temperature with the same initial conditions, presented in Harrington et al. (2020).

2. Experimental materials and method

2.1. Sample preparation

The samples were prepared using a 2015 batch of VOLCLAY MX80 granular bentonite powder obtained from Clay Technology AB and Svensk Karnbranslehantering AB (SKB), in Sweden. VOLCLAY MX80 is a trademark name of Amcol International Corporation (Hoffman Estates, IL, USA), which is a subsidiary of Minerals Technologies Inc. (New York, NY, USA). The VOLCLAY MX80 powder was acquired by Sibelco Nordic, who crushed and dried the powder before supplying it to Clay Technology and SKB. The chemical composition of the dry powder as supplied was SiO_2: 66.09%, Al_2O_3: 22.28%, Fe_2O_3: 4.39%, MgO: 2.44%, Na_2O: 1.87%, CaO: 1.54%, K_2O: 0.59%, SO_3: 0.58%, TiO_2: 0.19%, Cl: 0.01%, MnO: 0.01% (Svensson et al., 2017). The dry particle size of the majority of the powder (75%) was between 75 and 850 μm, with 15% having a smaller particle size than the range, and the remaining 10% being larger than 850 μm (American Colloid Company, 2001; Sibelco Sibelco, 2012). The mineralogy of the granular MX80 powder was 85% montmorillonite, which is part of the dioctahedral smectite group; the powder also contained 5% mica/illite, 4% quartz, 2% albite and minor quantities of cristobalite, tridymite, gypsum, calcite and pyrite (Svensson et al., 2017). The exchangeable cation data for this batch of the MX80 powder is given in Table S.1 the supplementary material. The chemical formula for VOLCLAY MX80 is $(Na,Ca)_{0.33}(Al_{1.67}Mg_{0.33})Si_4O_{10}(OH)_2.nH_2O$. The MX80 bentonite is being considered as a potential engineered barrier for use in the Swedish KBS-3 V disposal concept (e.g. Pusch, 1978; SKB, 1983, 2011). Following the methodology of Johannesson and Borgesson (1998) who were able to create uniform samples of similar dimensions to the test samples in this study, a specific weight of granular MX80 powder for a given sample length was wetted with the corresponding volume of distilled water to create test samples with a target dry density of 1.7 g/cm^3 and saturations of 92–100%. The wetted powders were then placed in a cylindrical-shaped steel vessel with a removeable base to provide radial confinement during compaction. They were then compacted with a steel bung under an axial load of 80 MPa for 24 h; the compaction pressure was slowly increased to the target value over more than an hour. The small space between the bung and the vessel, and between the vessel and its removable base provided a pathway via which the air could escape from the powder mixture during compaction. The first sample prepared was measured, weighed and dried without being tested, to ensure that the sample manufacturing procedure would produce identical samples with the target geotechnical parameters. This initial sample was found to have a dry density of 1.7 g/cm^3 and all subsequent samples were then made according to this procedure. Whilst bentonite behaviour is known to vary in relation to water chemistry and salinity, to isolate the effects of temperature on the system, distilled water was used both as the sample preparation fluid and the test permeant. Each sample was pressed for the same time period (24 h) and was manufactured to the specific starting length requirements of each test (Table 1). The samples were removed

Table 1
Starting sample dimensions and void length, pre-test geotechnical parameters, test temperature and test duration. The dry density was measured from a sample prepared specifically to obtain the geotechnical parameters; all subsequent samples were then made according to an identical procedure. The moisture content and saturation are calculated from the bulk and dry density. In all tests, the pore pressure was held at a constant 4500 kPa and the permeant used was distilled water.

Test	Sample length	Sample diameter	Sample mass	Bulk density	Dry density	Moisture content	Saturation	Void length	Test temp.	Test duration
	(mm)	(mm)	(g)	(g/cm^3)	(g/cm^3)	(%)	(%)	(mm)	(°C)	(days)
1	64.94	59.76	374.1	2.053	1.7	20.6	92	51.06	90	94.0
2	74.91	59.75	431.1	2.052	1.7	20.6	92	41.09	90	85.0
3	84.93	59.69	490.1	2.062	1.7	21.2	94	31.07	90	102.6
4	94.91	59.66	555.5	2.094	1.7	23.0	102	25.09	100	98.1

from the press using a piston and were turned down by ~0.6 mm in a machine lathe from their diameter after compaction (60.3 mm) so that they would fit snugly into the internal diameter of the testing apparatus without leaving gaps between the sample and the apparatus wall. The sample length was also machined down to be exactly the right starting length. To prevent unwanted swelling of the sample in advance of testing, the machine lathing was conducted under dry conditions, whilst care was also taken to minimise the loss of moisture from the sample through the use of plastic film and vacuum sealing. The sample weight and dimensions were recorded prior to the start of each test.

2.2. Experimental method

A custom-designed 316-stainless steel constant volume apparatus (Apparatus 1) that mimicked the borehole within a crystalline host rock as in the KBS-3V design (Harrington and Tamayo-Mas, 2016; Harrington et al., 2017, 2020) was used to conduct the first three experiments in this test programme (Fig. 1, upper half). Similar boundary conditions and test set-up were also used by Harrington et al. (2020) to investigate bentonite homogenisation at ambient temperatures (20°C ±1°). The fourth test presented in this paper took place in the newly commissioned apparatus (Apparatus 2), that had previously been used to conduct the vertically oriented ambient temperature tests presented by Harrington et al. (2020) (Fig. 1, lower half). This apparatus was manufactured from alloy-36 Steel (INVAR) which has a lower thermal expansion coefficient than 316-stainless steel. Apparatus 1 provided an internal length of 116 mm, whilst the internal length of Apparatus 2 was 120 mm; both apparatuses had a diameter of 60 mm (Fig. 1). The vessel used for the first 3 tests was instrumented with 5 load cells and 3 transducer arrays to measure the total stress and pore pressure respectively. The load cells used were button-type XF2041–3-2kN temperature-compensated devices supplied by StrainSense Ltd. The load cells were positioned on the outside of the pressure vessel and held in stainless steel housings. The force was translated from the clay to the load cells via tungsten carbide

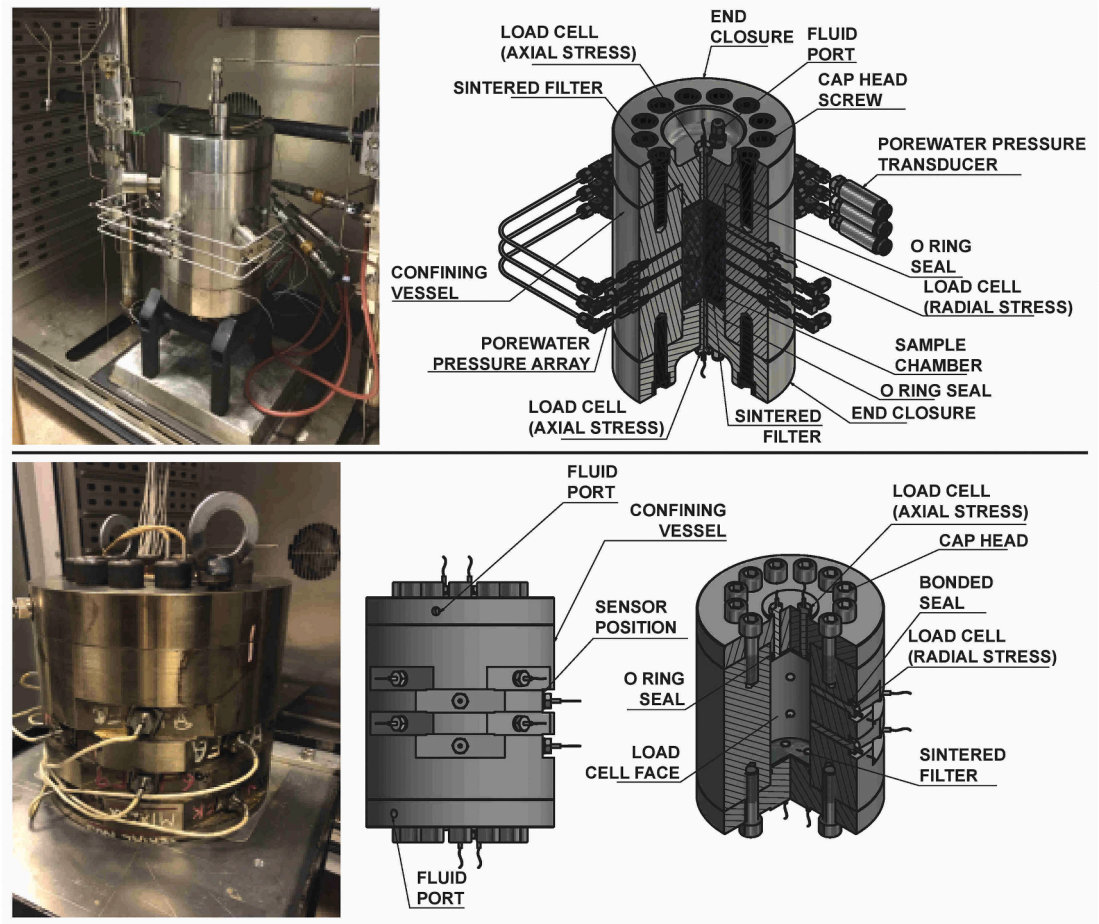

Fig. 1. Photographs and schematic images of the experimental testing apparatus for the first 3 tests (upper), and the INVAR apparatus used for the 4th test, showing the positions of the 8 radial load cells (lower).

pushrods, chosen for their hardness and incompressibility. The locations of the sensors on the surface of the sample with respect to the base of the vessel are indicated in Table 2 and are shown in the schematic found in the supplementary material Fig. S.1. The INVAR apparatus (used in Test 4) held 12 pressure sensors to measure total pressure (4 axial and 8 radial), but no pore pressure sensors. The pressure sensors used on the second vessel (XP1147-200BS temperature-compensated custom sensors supplied by StrainSense Ltd) did not require pushrods to translate the pressure from the clay to the outside of the vessel. Instead the instruments were screwed into the vessel and their face (containing a deformable membrane) touched the surface of the clay. A detailed description of this second apparatus is given by Harrington et al. (2020) (please also see supplementary Fig. S.2). The pressure measurements made by the load cells in Test 1 and 2 can be considered accurate to ±80 kPa, whilst the newer sensor type used in Test 3 and 4 can be considered accurate to ±15 kPa. The porewater pressure transducers were accurate to ±0.25% full scale range. The pore pressure measurement ports were fitted with small sintered filters to prevent clay material from migrating up the instrumentation holes. Large axial sintered filters (EC1 and EC2, supplementary Figs. S.1 and S.2) were also recessed into the end closures to ensure an even distribution of fluid entering the vessel at each of its ends; the test fluid was supplied to the sample using high precision syringe pumps (Teledyne ISCO D-Series 260D).

The whole pressure vessel assembly (excluding the syringe pumps) was stationed inside an oven (BINDER GmbH, Tuttlingen, Germany, Series FED 400) that had a temperature range of 5˚C above room temperature to 300˚C. At the start of the testing programme, the apparatus was calibrated. The calibration was carried out by placing a steel bung in the bore of the test vessel and filling the apparatus with the test fluid (distilled water). All of the tubework was carefully flushed with the test fluid through each available port to ensure no residual air remained, and the apparatus was heated to the testing temperature (Table 1). A pressure was then applied by one of the syringe pumps in 1 MPa increments from 1 to 7 MPa and back to 1 MPa. At each pressure increment, the pressure was held constant and the response on each of the sensors and on a Druck pressure calibration instrument was measured. As the sensor outputs were acquired as mV/V, a graph of sensor output against pressure measured by the Druck pressure calibration instrument was then used to provide a calibrated pressure output from each sensor (please see Tables S.2 and S.3 in the supplementary material). The load cells used in Apparatus 1 with the pushrod configuration showed a small amount of hysteresis due to friction between the vessel and the o-rings on the pushrod; the largest hysteresis observed during calibration occurred at higher pressures, and was most pronounced on load cell 4 at 6 MPa. The variation in pressure due to the hysteresis during the calibration of this apparatus was between 1 and 337 kPa across all load cells (please see Figs. S.3 and S.4, and Table S.4 in the supplementary material). This hysteresis was not present in Apparatus 2. After calibration, the oven temperature was reduced to ambient temperature, the steel bung was removed from the vessel and the tubework was carefully flushed again. The apparatus was then heated to the testing temperature before the commencement of the first test. The sample was pushed to the base of the void inside the apparatus and the remaining void space above the sample was filled with distilled water; the sample was not heated in advance of insertion because this would have affected the pre-test saturation. A detailed schematic of the experimental set up is shown in Fig. S.5 in the supplementary material. Distilled water was used as the external pressurising fluid in all of the tests performed.

A pore pressure was carefully applied alternately to each end of the sample in 500 kPa steps to the target value of 4500 kPa, starting at the end of the apparatus that was originally void space. This kept the sample fixed against the other end of the apparatus interior and prevented it from sliding along the bore of the vessel before the sample swelling began. The pore pressure reference value was chosen for comparability with the current Swedish repository concept in collaboration with the SKB radioactive waste management company. The flow rate into and/or out of the sample was then controlled and monitored using the syringe pumps and a single digital control unit. Each pump was operated in a

Table 2
Test and apparatus numbers, and corresponding sensor locations. Porewater pressure is abbreviated as PWP above. The values quoted for 'Rotation around vessel' for the porewater pressure sensors describe the positions of the four point measurements that provide the average porewater pressure measurement for the given porewater pressure array number. The final swelling pressures are averaged over approximately the last six hours of test data.

Test	Apparatus number	Pressure Sensor	Distance from vessel base	Rotation around vessel	PWP Array	Distance from vessel base	Rotation around vessel	Peak swelling pressure	Final swelling pressure
			(mm)	(˚)		(mm)	(˚)	(kPa)	(kPa)
1	1	A1	0	–	–	–	–	1533	753
		R2	15.2	0	1	36.6	0, 90, 180, 270	927	785
		R3	58	120	2	58	0, 90, 180, 270	1731	146
		R4	108.2	240	3	79.4	0, 90, 180, 270	–	–
		A5	116	–	–	–	–	–	–
2	1	A1	0	–	–	–	–	4074	1193
		R2	15.2	0	1	36.6	0, 90, 180, 270	1035	1028
		R3	58	120	2	58	0, 90, 180, 270	485	471
		R4	108.2	240	3	79.4	0, 90, 180, 270	–	–
		A5	116	–	–	–	–	–	–
3	1	A1	0	–	–	–	–	2477	1465
		R2	15.2	0	1	36.6	0, 90, 180, 270	3909	1145
		R3	58	120	2	58	0, 90, 180, 270	2325	833
		R4	108.2	240	3	79.4	0, 90, 180, 270	391	279
		A5	116	–	–	–	–	456	394
4	2	A1	120	–	–	–	–	1156	1172
		A2	120	–	–	–	–	866	850
		A3	0	–	–	–	–	7367	2126
		A4	0	–	–	–	–	8424	2209
		R1	96	0	–	–	–	1011	1005
		R2	96	90	–	–	–	2621	1596
		R3	72	45	–	–	–	3707	1794
		R4	72	135	–	–	–	1087	1097
		R5	48	0	–	–	–	2155	1802
		R6	48	90	–	–	–	2898	1794
		R7	24	45	–	–	–	6365	2241
		R8	24	135	–	–	–	4269	1902

constant pressure mode and thus the flow rate and direction were not prescribed. Inflow or outflow could therefore occur at either end of the test vessel. The syringe pumps had a resolution of 16.63 nL and were controlled by a microprocessor that continuously monitored and adjusted the pump volume. The volumetric control system for each pump was factory calibrated. Once the pore pressure had been applied to the sample, no external hydraulic gradient was then applied to the clay at any further point in the test. FieldPoint™ and cRIO logging hardware and the LabVIEW™ data acquisition software (National Instruments Corporation, Austin, TX, USA) were used to log the flow rate, total stress and pore pressure at 2 min intervals, providing a detailed time series dataset. Over the duration of the test, the sample was able to swell into the initial void space (see supplementary Fig. S.5). Each test was run for a sufficient time to delineate the swelling response (Table 1), allowing comparison between the tests. At the end of each test, the pressure was incrementally reduced at both ends of the vessel at the same time to ensure that there was no hydraulic gradient placed across the sample. Once the pressure had reduced to 70 kPa, the pumps were stopped, although the sample still had access to a reservoir of water at each end. The oven was also switched off, but remained closed for a minimum of 16 h whilst the temperature reduced to ambient. The sample was extruded out of the vessel in increments and sliced into approximately 10 mm thick pieces using a sharp blade. The slices were weighed immediately after their extrusion, whilst the remainder of the sample still in the vessel was covered with clingfilm to minimise moisture loss. The weighed slices were placed in an oven at 105˚C and dried to determine the moisture content. Friction, caused by swelling of the clay during testing, resulted in trace amounts of material being left on the vessel wall during the extrusion. However, as this was a very small proportion ($\leq$0.25 mm) of the overall diameter (60 mm), it is not likely to have influenced the moisture content results. The post-test dry density (ρ_d) was calcuated from the moisture content for each sample assuming full saturation using a specific gravity of 2.77 (Wang et al., 2013), a pore fluid density of 1000 kg/m^3 and assuming a saturation of 1. This is a reasonable assumption because the start saturation of the samples was close to unity and the void was filled with water.

3. Results

3.1. Development of swelling pressure

The load cell values recorded throughout the duration of each test showed a similar and generalised pattern, though there was significant variance between the load cell values present throughout all of the tests. The value recorded by each of the sensors except those closest to the top of the vessel peaked within the first 10 days of testing. The peak value was generally larger the lower down the vessel the sensor was located (please see Fig. S.6 in the supplementary material for the peak and final swelling pressures as a function of sensor position). Over the course of a test, the recorded pressures tended to converge, however, significant variance still existed when the tests were terminated, despite the stresses and pore pressures reaching almost steady values (Fig. 2). The strength of the response was more pronounced in tests where the sample-to-void ratio was smaller. In addition, the pressures measured at the base of the vessel were always higher and the values decreased towards the top of the vessel. This trend was not quite the case for every sensor in every test at all times, where some overlap (e.g. Test 1 Axial 1 and Test 1 Radial 2 at later times, and some of the Test 4 sensors positioned on the same plane) was occasionally seen. A detailed graph of the outputs from every sensor can be seen in the supplementary material (Fig. S.7). The swelling pressure was defined as the total stress minus the pore pressure. It should be noted that the calculation of swelling pressure assumed that pore pressure was uniform along the length of the apparatus. This assumption is valid for parts of the sample that expanded into the void space in the vessel. During the early stages of the test, for sensors located next to the pre-compacted clay, it is likely that total stress rather than swelling pressure was recorded. However, the rapid increase in the radial stresses suggested that the clay had access to water within the first couple of days (Fig. 2B). In the first test, the axial load cell A1 initially peaked at a swelling pressure of 1540 kPa but dropped to values in line with radial load cell R2 within 15–20 days (Fig. 2A). The swelling pressure recorded in this radial load cell (R2), which was located at the bottom of the vessel where the sample was positioned at the start of the test, rose to a peak value of 930 kPa very early in the test (within the first few hours). This swelling pressure then decayed to an approximately constant 700 kPa. Towards the end of the test, as the test fluid penetrated further into the clay sample and the sample swelled, the swelling pressure recorded by

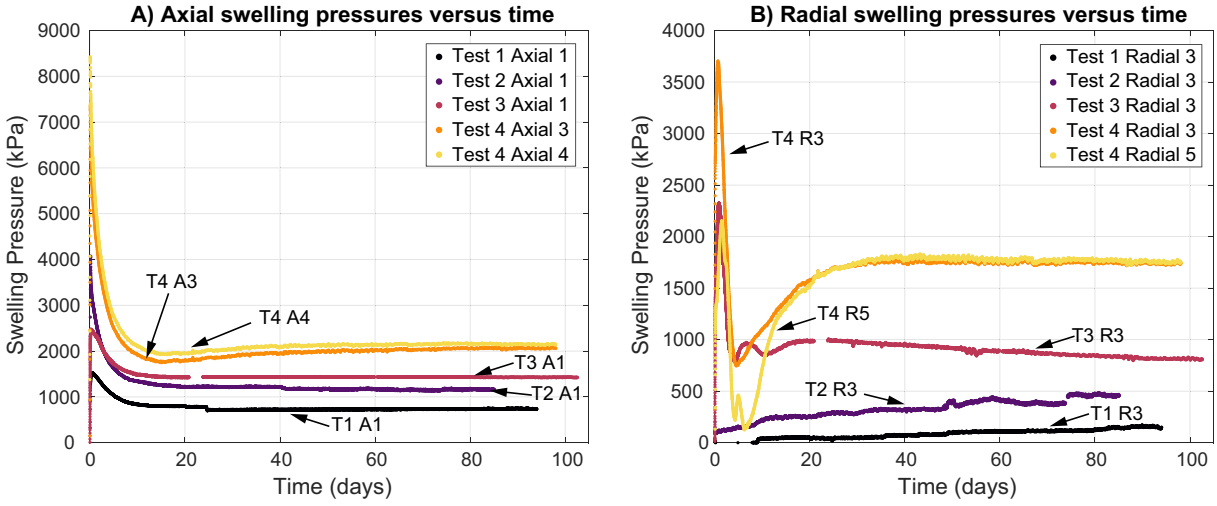

Fig. 2. Swelling pressures over the duration of each test measured by A) axial and B) radial swelling pressure sensors assuming a pore pressure of 4500 kPa. A) The axial data are for the axial 1 load cell (Tests 1–3) and the axial 3 and 4 load cells (Test4) located at the base of the pressure vessel and immediately adjacent to the sample at the start of the test. B) The radial data are for radial load cell 3 (Tests 1–4) and radial load cell 5 (Test 4). Radial load cell 3 in Tests 1–3 was located at the lengthways midplane of the vessel. In Test 4, the configuration of the load cells was such that no sensor was exactly on the midplane, but radial load cells 3–6 were spaced an equal distance either side of it, with 3 and 4, and 5 and 6 on the same planes (Please see Fig. S.2 in the supplementary material). Thus one load cell from each plane was chosen (radial load cells 3 and 5).

radial load cell R3 located at the vessel midplane began to increase (Fig. 2B). Given the rate of swelling pressure increase recorded by R3, it was clear that it would take many months for the value to reach that of the other radial load cell, if this happened at all. Unfortunately both radial load cell 4 and axial load cell 5 stopped functioning and were unable to give data over the duration of the test. The swelling pressure traces evolved in a smooth manner and there were no large inflections indicative of discontinuous frictional behaviour (stick-slip phenomena). However, continuous friction will still have occurred between the sample and the vessel wall. Based on the observations from the experiments presented in this study and those of (Dueck et al., 2016), the friction angle was likely to be relatively small.

As was observed in the first test, the second test showed significant variance between the recorded stress values throughout the test duration until its termination at 85 days. The axial load cell 1 peaked at 4060 kPa then dropped to values similar to (although slightly larger than) those of radial load cell R2 within 15–20 days. Radial load cell R2 peaked at a swelling pressure of 1030 kPa then dropped to ~950 kPa by day 8 and remained approximately constant for the rest of the test. Similarly to Test 1, radial load cell R3 showed lower swelling pressures throughout the test that rose very gradually to a maximum of 480 kPa close to the end of the test, presumably as water progressively seeped into the centre of the sample and the sample continued to homogenise. The data from radial load cell R4 and axial load cell A5 again was not able to be interpreted because they recorded a significant drift. Thus at the end of the second test, the decision was made to replace all three radial load cells and the axial A5 load cell at the top of the vessel with the new type of pressure sensor already employed on Apparatus 2. The new type of sensor was able to make swelling pressure measurements directly from the face of the clay and therefore eliminated any effects of hysteresis that might have been present in the data. In Test 3, the maximum swelling pressure was recorded by radial load cell R2, which peaked right at the start of the test and then steadily decayed until the test was terminated at day 102 (please see Fig. S.7 in the supplementary material). The axial load cell next to the clay specimen at the test start (A1) peaked at a lower swelling pressure (2500 kPa; slightly above the peak of the radial load cell R3) and then, like sensor R2, steadily decayed to a constant value. Between day 10 and day 15, the swelling pressure value measured by the axial load cell A1 surpassed that recorded by the radial load cell R2 and from that point until the end of the test, recorded the highest swelling pressures. Axial load cell A5 and radial load cell R4 recorded the lowest swelling pressure values, gradually rising from 0 to 500 kPa over the first 30 days of the test, and then maintained a constant value until the end of the test.

All tests showed that the development of swelling pressure was spatially complicated and there was significant anisotropy in the response. This was especially highlighted by the data from Test 4 (Fig. 3) where, at 4 positions along the length of the sample, the radial swelling pressure was measured at two points 90 degrees from each other on the same plane (please see Fig. S.2 in the supplementary material). The difference between the swelling pressure measurements made on these planes provided information about orthogonal stresses acting perpendicularly in the sample at those positions of measurement along the length of the sample. The average axial and radial swelling pressures at each plane along the sample length and the difference in the orthogonal pressures on those planes were both examined. The difference in orthogonal pressures were largest in the early stages of Test 4, but quickly became similar for each plane of measurement (within ~20–30 days) (please see Fig. S.8 in the supplementary material). The peak values of orthogonal pressure can be seen clearly at early times in Fig. S.9 in the supplementary material, whilst the average axial and radial swelling pressures are shown in Fig. S.10. The average radial and axial swelling pressures for all tests can also be seen in the supplementary material (Fig. S.11). The large differences in orthogonal pressures observed at early test times are thought to have occurred because of very small differences in the starting sample dimensions, which may have

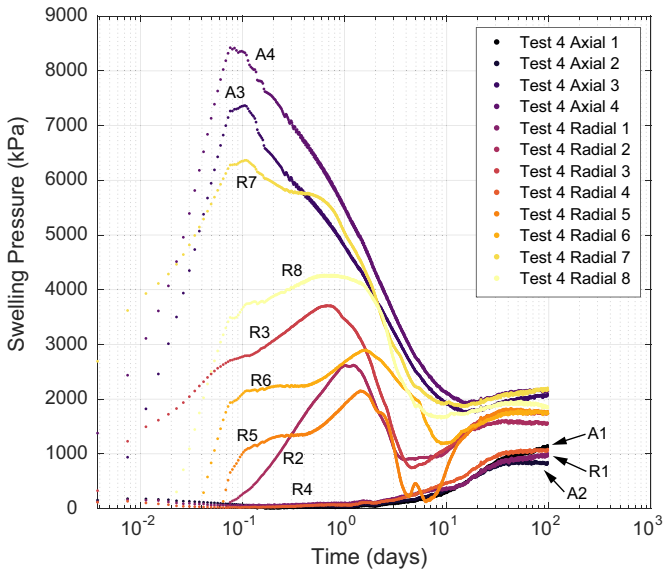

Fig. 3. Swelling pressures over the duration of Test 4 measured by the axial and radial swelling pressure sensors, highlighting the peak values at early times in the test history.

caused the sample to contact differently on the individual sensors whilst also influencing both the initial fluid migration and the absolute values of peak stress in the early stages of testing. These heterogeneities in the starting conditions should have been rapidly negated however, due to the fast swelling response of the the bentonite.

There was still a significant difference between the maximum and minimum recorded swelling pressures in each test at the end of testing, and the rate of change of swelling pressure after about 20–30 days in each of the tests was small. This showed that the bentonite was able to use its internal shear strength (Gilbert et al., 1996; Stark and Eid, 1996; Fox et al., 1998; Fox and Stark, 2015) to maintain the differential stresses for long periods of time, which may have impacted rates of homogenisation. In addition, where information from axial load cell A5 (at the top of the apparatus) was available, the data showed either a peak (Test 3) or the data was approaching an asymptote (Test 4) by about 30 days of testing. Together this suggested that the sample had swelled to completely fill the initial void by this time in the test, and from this point onwards, internal reorganisation of the clay and fluid distribution within the sample was occurring up until the point that the test was terminated. It also indicated that if the samples had swelled to completely fill the start void within 30 days and significant anisotropy in the swelling pressure data was still extant at 100 days, homogenisation of the full length of the sample would take a very long time to occur (if it occurred at all). There was also a correlation between the peak swelling pressure and the initial void length of each test (Table 3), although it should be noted that peak values of swelling pressure are sensitive to the initial conditions, as well as the availability and migration of water through the sample. For longer initial void lengths (equating to shorter starting samples), both the peak and the end-of-test swelling pressures were smaller. This result was expected because the test with the shortest starting sample had the least clay material within the test vessel and had the lowest average final dry density, thus the reduced quantity of clay would have been able to exert less of a force on the walls of the vessel compared with a starting test sample that had originally been longer. The axial peak value in Test 3 was much lower than expected based on the data from the other three tests and previous observations (Harrington et al., 2020) (Table 3, and please also see Fig. S.6 in the supplementary material) and it is thought that this was the result of a slight shift in the sample positioning away from the base of the vessel at the start of the test. For a sodium bentonite with a dry density of 1.7 g/cm^3

Table 3
The peak swelling pressure measured during each test and the sensor that the peak value occurred on. Tests 1–4 give data from this study and Tests 1A-3A are the data from Harrington et al. (2020). The 'Axial base', average swelling pressures and cumulative flow data are calculated from the end-of-test values. For the sake of comparison, only sensors R2 and R3 were used to calculate the average radial swelling pressures for Tests 1–3; in Test 4, all 8 radial load cells were used to calculate the averaged value. The amount of swelling as a percentage attributed to fluid uptake from the base of the vessel is calculated by dividing the cumulative inflow volume adjusted for the thermal expansion of water at the testing temperature, by the starting void volume. This then allows the amount of swelling due to fluid absorption from the void space into the clay to be estimated ('Swelling at void'). The average dry density values are for the post-test sample.

Test	Peak axial	Peak radial	Axial base	Average axial	Average radial	Cumulative inflow	Cumulative outflow	Swelling at void	Average dry density
	(kPa)	(kPa)	(kPa)	(kPa)	(kPa)	(mL)	(mL)	(%)	(g/cm^3)
1	1533 (A1)	927 (R2)	732	–	452	33.99	30.74	76.46	0.913
2	4074 (A1)	1035 (R2)	1160	–	729	25.97	23.03	77.65	1.062
3	2477 (A1)	3909 (R2)	1424	904	961	26.07	23.13	70.32	1.182
4	8424 (A4)	6365 (R7)	2107	1545	1608	29.24	8.59	58.78	1.334
A	2647 (A4)	3307 (R6)	306	237	187	36.5	34.9	76.6	0.843
A	3844 (A4)	2737 (R6)	512	328	327	31.0	28.7	75.7	0.992
A	3948 (A3)	4213 (R6)	816	544	674	28.1	26.0	71.6	1.147

exposed to pure water, a swelling pressure in excess of 16 MPa is expected at 100% saturation and ambient temperature (Karnland et al., 2006); however, it should also be noted that the swelling pressure is both stress-path dependent and affected by the measurement method, with isovolumetric methods providing intermediate values (Sridharan et al., 1986). Whilst the starting sample in each test had a dry density of around 1.7 g/cm^3, as the sample expanded the dry density of the material would have evolved to lower and lower values. In addition to this, at elevated temperatures bentonite swelling pressures may be expected to be lower (e.g. Pusch, 1980; Villar and Lloret, 2004), although the reverse result has also been seen (e.g. Pusch et al., 1990). Every sample's peak swelling pressure was significantly lower than 16 MPa (Table 3), with the peak axial and radial swelling pressures for the longest tested sample (Test 4: 90 mm) being the highest. This suggests that the reduced peak values observed reflected the decrease in dry density and increase in moisture content as the sample expanded into the void space.

3.2. Water uptake

The flow of distilled water into and out of the testing vessel was measured in each test (Fig. 4) and a well-defined transient was recorded. The most significant rate of inflow to and outflow from the vessel in each of the tests occurred in the first 20 days of testing. The cumulative flow curves were adjusted to account for the thermal expansion of water entering the testing vessel at an elevated temperature from the syringe pumps at an ambient temperature, using a thermal expansion coefficient of 2.1×10^{-4} °C^{-1} (Tennent, 1971). The flow rate curves were nearly symmetrical and the magnitudes of the in- and outflows were approximately equal in Tests 1 to 3, indicating that the overall change in volume in the vessel was very small in these tests. This is in contrast to Test 4 where the inflow was substantially larger than the outflow, and does not appear to have reached a steady state. In Test 4, the syringe pump connected to the top of the vessel initially recorded a volume decrease suggesting that fluid was flowing into the sample. At day 1.4, the observed inflow reversed, with the pump recording an outflow until approximately day 35. Between day 35 and day 45 the volume flux was near-constant. From day 45 for the remainder of the test, the pump recorded a very gradual inflow at a rate consistent with the observations made from the pump at the top of the vessel in Test 1. This pattern of behaviour of inflow followed by outflow seen in the early test stages at the pump connected to the top of the vessel in Test 4 was inconsistent with the observations made from the same pump in the other 3 tests. After day 1.4, the form of the outflow curve in Test 4 was consistent with the other test outputs, although the magnitude of the values would have been expected to match those of the other syringe pump. It is not clear what caused the reverse in the direction of flow at the pump connected to the top of the vessel in Test 4, although it is possible that a leak from the outflow pump was causing the volume recorded in the pump to be smaller than it should be.

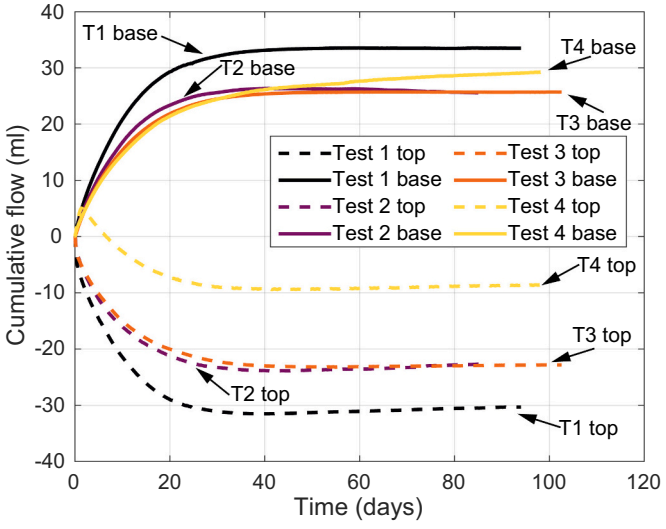

Fig. 4. Cumulative flow into the testing vessel from its base and out of the vessel at the top of the apparatus.

During Test 1, accounting for the thermal expansion of water, 33.99 mL of water entered the sample through the base of the vessel, which was a much smaller volume than that of the start volume of the void (144.4 mL), and equated to a 23.5% the volume change due to swelling driven by water influx to the base of the test sample (Table 3). The remainder and majority (76.5%) of the volume change occurred through unconstrained swelling at the top of the sample into the void space. Both the intake of water at the base of the vessel, and the upwards swelling of the sample into the void space caused water to outflow through the top of the vessel. In Test 2, 25.97 mL entered the sample through its base, which was equivalent to a 22.4% contribution to the closure of the initial void (116.18 mL). This value was lower than expected compared to the data from the other tests in this study, especially when contrasted with Test 3 where the sample took 26.07 mL of fluid through the base, equating to 29.7% of the volume required to close the initial void volume (87.85 mL). The cumulative volumes of both inflow and outflow may have been smaller in Test 2 because the test duration was shorter than for the other tests. However examining the form of the inflow and outflow curves (Fig. 4) showed that after about day 50, the pump at the base of the vessel began to very gradually take in fluid from the sample, whilst the pump connected to the top of the vessel started feeding fluid into the vessel, i.e. the flow directions were reversed. It is not clear therefore that additional test length would have resulted in any increase to the cumulative inflow or outflow volumes. In the final test, where the

starting sample was longest, the cumulative inflow was 29.24 mL, which represents a 41.2% contribution to the closure of the volume in the void space (70.94 mL), meaning that 58.8% of the closure occurred through the swelling of the top surface of the clay sample. The observation that the majority of the swelling occurred from the top of the sample upwards into the void space, was supported by the measurements of moisture content made along the length of each of the post-test samples (presented in subsection 3.4).

3.3. Development of pore pressure

That the expansion and swelling of the clay in each test occurred in a gradual and consistent manner, was supported by the pore pressure data (Fig. 5). For pore pressure arrays 1 and 2, the filters connected to these transducers were located next to the sample at the start of each test. Pore pressure array 3 was located closest to the top of the vessel and at the start of Tests 1 and 2, it was adjacent to the initial void space; thus the pore pressure array 3 registered the pressurised test fluid immediately. Array 3 continued to read the 4500 kPa pore pressure for the entire duration of both of these tests (Tests 1 and 2). In Test 3 where the starting sample was longer (85 mm), pore pressure array 3, like arrays 1 and 2 in all of the tests, was obstructed by the starting sample. As the test fluid moved into the clay and the clay expanded up into the initial void space, this sensor array began to register a pressure. For array 3 in Test 3 this happened between day 6 and 7 (Fig. 5). To elucidate the pore pressure behaviour at early times in the experiments, only the first 30 days of experimental data were presented in Fig. 5. The pore pressure data for each of the sensors over the complete testing period can be seen in the supplementary material (Fig. S.12).

In all the tests, because the sample obstructed the transducers from seeing the pore pressure in both arrays 1 and 2 when it was first applied to the sample, no immediate pressure change was recorded by these two transducers. Array 2 (located at the midplane of the vessel) was the next to see the applied pore pressure in all three tests. Array 2 saw the applied pore pressure signal at the soonest time in Test 1 (6 days) and latest in Test 3 (13–14 days). The pore pressures reached Array 1 (the array closest to the base of the vessel) last in all of the tests; as with Array 2, the applied pore pressure signal was observed at the earliest time in Test 1 (12 days) and the latest time in Test 3 (between 21 and 24 days). Once the pressure recorded by each sensor reached the applied pore pressure, the recorded value remained constant for the rest of the test.

3.4. Post-test moisture content and dry density

At the end of the testing period (approximately 100 days) each sample was removed from the testing vessel and subsampled to give information on the moisture content as a function of the sample length. During the testing period, each of the samples had swelled to completely fill the internal volume of the vessel, although there was a large difference in the consistency, water content and density of the material between the top and bottom of the sample. The low density and strength of the upper part of the specimens meant that it was only possible to obtain accurate subsamples by mass and not volume. Each of the samples was removed from the test vessel incrementally using a hydraulic ram to extrude the sample. The material was subsampled with a knife to obtain cylindrical portions of the test sample that had the diameter of the vessel and were approximately 10 mm in length. These portions were immediately weighed and placed in an oven to dry at 105°C. Because the sample had swelled radially against the vessel walls during the test period, a hydraulic ram was required to extrude the sample. All of the samples experienced a large amount of swelling and they all produced post-test samples that were similar in that there was not much variation in the moisture content in the first half of the sample, from its base to approximately the midplane. In all of the tests, the moisture contents were significantly higher at the top of the sample, and showed large gradients in the region of the internal vessel volume that would have been void space at the start of each test. The starting moisture content of the pre-test samples is given in Table 1; Fig. 6 A shows that the post-test samples absorbed a minimum of 2–3 times the starting moisture content, and the minimum post-test moisture contents were found through much of the space originally occupied by the start material.

There is a correlation between the length of the starting sample and final moisture contents throughout the post-test sample; the samples that had a longer starting length had lower moisture contents at all points along the sample length. This is unsurprising because the increased volume of clay in the vessel at the start of the test would have needed to absorb a smaller amount of water at either end to induce enough swelling in the material to close the void space. These longer samples also show a trend for smaller moisture content increases in the part of the interior of the vessel that would have been void space at the start of the test. As expected, the same correlations in the moisture content data are observed in the dry densities (Fig. 6 B); samples with longer starting lengths had higher final dry densities at all points along the length of the sample. Also, the increase in sample length correlates with an increase in dry density in the part of the interior of the vessel that was originally void space at the start of the test. There is very little change in the moisture content or dry density within each sample over the first 60 mm from the sample's base. Based on the distribution in moisture content along the axis of the sample, the system would appear to be in a transient state where homogenisation times may be considerably longer. The rate of water uptake by the sample is very slow resulting in the large differential in axial stress measured between the top and bottom of the apparatus at the end of the test period (please see Test 3 in Fig. S.7C in the supplementary material). This is in line with the observations made by Harrington et al. (2020) for their test samples, which were similar to these tests but conducted at ambient temperature.

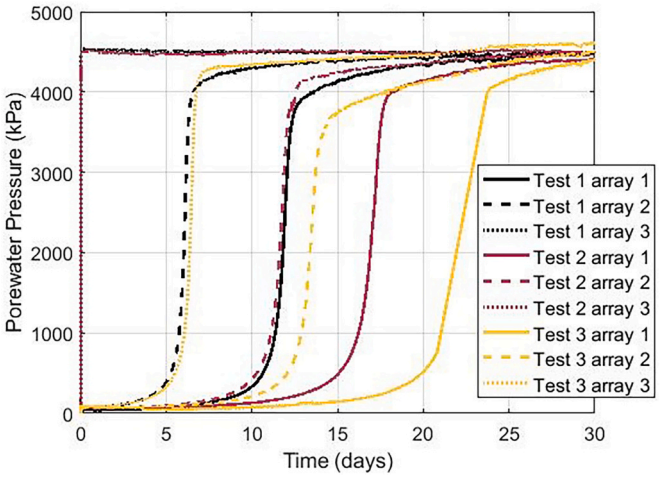

Fig. 5. Pore pressures measured by the three radial transducer arrays over the first 30 days of each of the tests.

4. Discussion

These experiments have shown that at an elevated temperature of 90°C, as in the ambient temperature case (Harrington et al., 2020), bentonite can swell into an engineered cavity, occupying the void and creating a swelling pressure on each end of the confining vessel. This is an encouraging result in terms of the usage of bentonite as an engineered barrier for HHGW disposal. There are strong similarities between the results at elevated temperature with their ambient temperature counterparts, and the patterns observed within the data are comparable; however there are also some notable differences. The data recorded in these experiments demonstrate that the swelling pressures within the samples are not uniform over the sample length and are continually evolving over the duration of the test. The tests have also shown that,

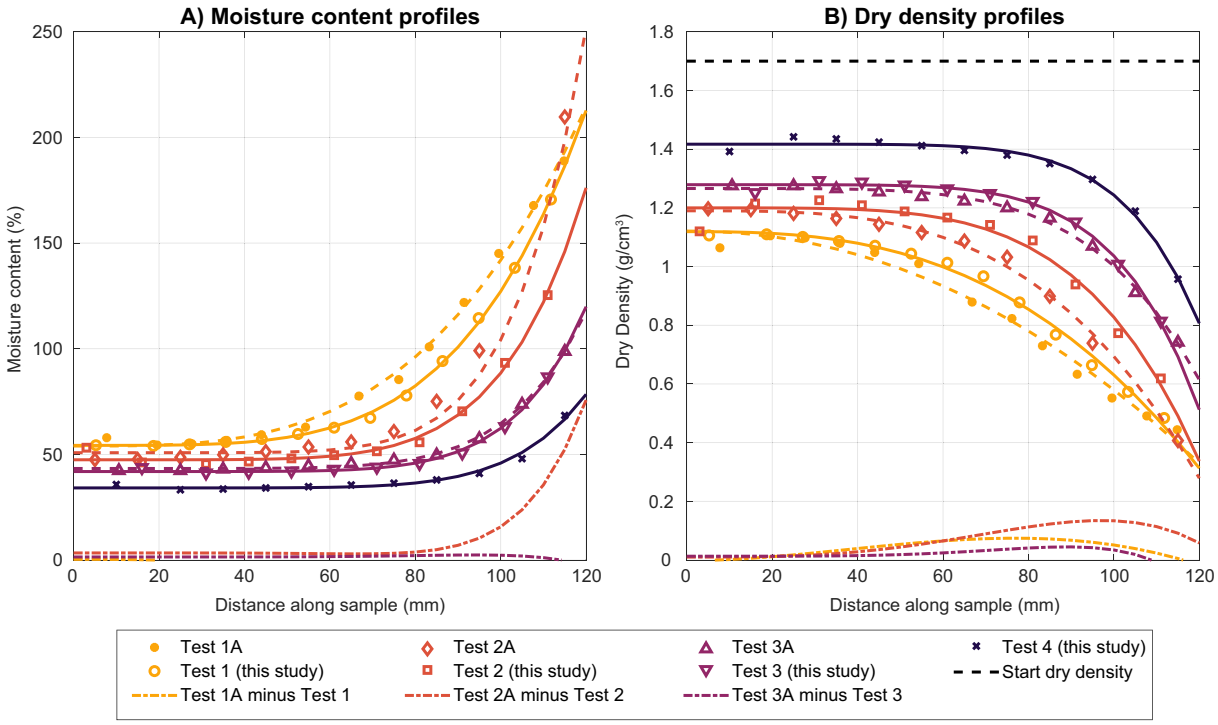

Fig. 6. Comparison between A) the post-test moisture content data and B) the dry density, with power law fits for the four tests of this study (Tests 1–4, elevated temperature, solid lines) and the ambient temperature tests of Harrington et al. (2020) (Tests 1A-3A, dashed lines). The difference between the two power law fits for each test pair is indicated by the dot-dashed line. There was no 95 mm ambient temperature test to compare with Test 4 of this study.

with the exception of the peak axial data from Test 3, there is a positive correlation between sample length and both the peak and the average end-of-test swelling pressures. For longer samples the volume of clay inside the vessel was increased. This increased the sample's post-test average dry density, and this contributed to the larger peak and average end-of-test swelling pressures seen (Table 3, Fig. 7). These relationships can also be seen plotted against void length in the supplementary Fig. S.13. For three of the tests, the largest peak swelling pressure value was recorded on the axial load cell at the base of the vessel. In contrast however, the largest peak swelling pressure in Test 3 was observed on the radial load cell R2. Given that the sample manufacture was identical for each test sample, and much effort was put into ensuring that the material was completely mixed before compaction, it is unlikely that significant sample heterogeneity existed between the test samples. It therefore seems probable that this difference in swelling pressure is primarily due to a slight shift in the placement of the sample away from the end of the vessel during pressurisation.

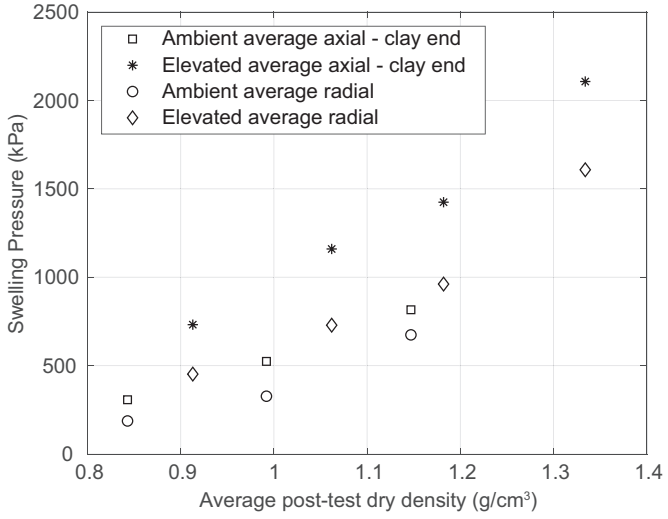

Fig. 7. The averaged end-of-test swelling pressures (axial and radial) plotted against the averaged post-test dry density of the sample. The swelling pressures were calculated from approximately the last six hours of data. Only the axial sensor at the base of the vessel was used because the axial data from the top of the vessel was not available in some of the tests.

The data from the experiments presented in this paper haven been compared with the recently published results of Harrington et al. (2020). In their tests, Harrington and co-authors present the results of similar tests conducted at ambient temperatures. The first three of their tests (hereafter referred to as Test 1A, Test 2A and Test 3A) are the most relevant for comparison because they were also conducted in a vertical orientation with sample lengths of 65, 75 and 85 mm used (corresponding to post-test averaged dry densities of 0.843, 0.992 and 1.147 g/cm^3 respectively); these tests compare directly with Tests 1–3 in this paper (see Table 3 for the post-test averaged dry densities from this study, and Fig. 6B for the dry density gradients). The development of swelling pressure in the elevated temperature tests is clearly different to that observed under ambient temperature conditions (Fig. 8). Comparative data for Test 1 and Test 1A are shown in Fig. 8; data for all of the tests can be seen in Fig. S.14 in the supplementary material. While peak values of axial and radial pressure were lowered under a thermal load, asymptotic values were considerably higher than those observed under ambient conditions (Fig. 7). The peak swelling pressures of the elevated temperature tests presented here were lower than for the ambient temperature counterparts; the elevated temperature peak swelling pressures were 57.9% and 62.7% respectively of the swelling pressures from the equivalent 65 mm and 85 mm tests of from Harrington et al. (2020). The peak swelling pressure of the 75 mm elevated temperature test (Test 2) is anomalously high in the context of the two sets of experiments and is 106.0% of the ambient temperature (Test 2A) peak swelling pressure. This can be seen clearly in Fig. S.13 in the supplementary material. The reason for the large peak in Test 2 is unclear. In addition, the average swelling pressures observed compare well with the

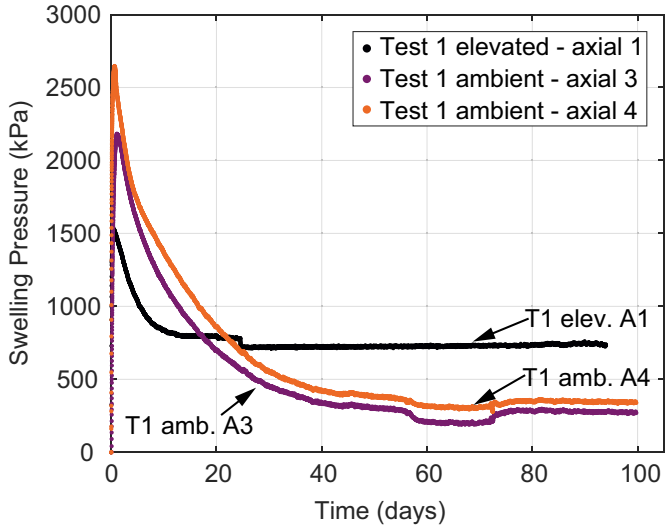

Fig. 8. Comparison between the axial swelling pressure measured at the base of the vessel in Test 1 presented in this study and those conducted at ambient temperature and presented in Harrington et al. (2020) (Test 1A), assuming a pore pressure of 4500 kPa. A direct comparison between Test 1 of each dataset can be made as the test geometries were the same in each case, and in each test the same starting sample length (65 mm) was tested.

experimental observations made in axial swelling tests by Dueck et al. (2016, 2019). The averaged swelling pressure data for Tests 1 and 2 with much lower averaged post-test dry densities (Table 3) were unfortunately not available due to the failure of the R4 and A5 sensors. However, for the data available and akin to the Dueck et al. (2019) data, this study shows slightly higher average swelling pressures when compared to the MX80 model of Börgesson et al. (1995) and slightly lower average swelling pressures than those expected by the model of Akesson et al. (2010), which was derived from the experimental results of Karnland et al. (2006). These comparisons therefore suggest that after the test period, the elevated temperature bentonites are at least as homogenised as their ambient temperature counterparts.

There is limited high quality swelling pressure data describing the hydromechanical behaviour of bentonites at high temperatures. Many authors have reported seeing a decrease in swelling pressure with increasing temperature (Pusch, 1980; Lingnau et al., 1996; Villar and Lloret, 2004; Tang and Cui, 2005; Ye et al., 2014; Tripathy et al., 2017), though there have also been studies presenting the reverse (Karnland et al., 1994; Börgesson et al., 1995). The observations of Ye et al. (2014) were made on compacted GMZ01 bentonite samples; no void space was included in their tests. In their tests, the measured axial swelling pressure showed a decreasing trend for increasing temperature up to 80°C (the highest temperature tested) (Ye et al., 2014). The same trend for decreasing swelling pressure with increasing temperature has been observed in Na-bentonite-sand mixtures for a temperature range of 26–100°C (Lingnau et al., 1996), and in MX80 tests (measuring suction pressures) for a range of salt solutions (Tang and Cui, 2005). The data presented by these authors are single points for each test. Pusch (1980) predicts a 50% decrease in swelling pressure when the temperature is elevated from 20°C to 90°C; in his experiments, he specifically studies the second maximum after the first peak, equivalent to the end-of-test swelling pressures presented here. This data is in direct contrast with the observations made in this study, where the elevated temperature produces higher final swelling pressures than for equivalent tests conducted at ambient temperature (Harrington et al., 2020) (Fig. 7). On the other hand, Pusch et al. (1990) observed that swelling pressures of Na-bentonites in contact with distilled water increased with temperature, unless the material had a high dry density of about 2 g/cm^3, and in which case no change was observed. Conflicting observations are also provided by the permeability measurements at elevated temperature made by Daniels et al. (2017), who recorded a decrease in permeability with increasing temperature above 60°C, which the authors partly attributed to the reduction in pore volume due to sample consolidation. The total stresses showed an increase in the asymptotic stress value after each increase in temperature up to 150°C, and a positive correlation between the maximum total stress value at each temperature step, consistent with the data from this study. However, the trend in the average effective stress with increasing temperature was less clear. The first test showed a decrease in average effective stress with increasing temperature, whilst the second test showed the same trend above 90°C on the radial sensors and above 120°C on the axial sensors. This also contributed to the hypothesis of thermal consolidation of the test samples and is at odds with the data from this study, but the much lower sample density in these tests compared to those of Daniels et al. (2017), may mean that their observations have limited impact on the results presented here. The experimental configuration in the Pusch (1980) experiments did not include a void space, and the dry densities tested (1.75–2.2 g/cm^3) were also significantly higher than the sample dry densities presented here (Fig. 6 B), which may account for the differences in behaviour in results to those performed on single density samples (e.g. Pusch, 1980; Lingnau et al., 1996; Tang and Cui, 2005; Ye et al., 2014; Daniels et al., 2017).

The elevated temperature tests presented here also showed that the transient response of the peak stress was shorter than it was in the ambient temperature equivalent (Fig. 8); in the elevated temperature tests the swelling pressure curve showed a more accelerated increase and decrease in stress, whilst the form of the ambient temperature curves was much more broad. It took longer for the swelling pressures to reach an asymptotic value in the ambient temperature tests than it did for the elevated temperature experiments. This is an important observation regarding the use of bentonite buffers around the waste canisters in radioactive waste disposal concepts, where elevated temperatures created by the waste are expected to occur early on as the buffer is also hydrating. Provided that there is available groundwater and that the groundwater is not driven away from the canister due to the temperature gradient, the bentonite will more quickly swell to fill cavities in and around the buffer at higher temperatures than it would at an ambient repository temperature. In turn, this could help the buffer seal more quickly around the waste preventing any further egress or migration of fluids; this is more likely to occur in the far-field and further away from the waste packages. In a radioactive waste repository, a gradient in temperature will also exist between the heat emitting waste and the cooler host rock. A clear response in bentonite hydro-mechanical behaviour has been observed in samples subjected to a thermal gradient (Tripathy et al., 2017); next to the heat source, drying and shrinkage of the bentonite is seen, with a redistribution of the water to lower temperature areas. The geometry of the tests presented by Tripathy et al. (2017) also yielded a reduction in the density of the bentonites at the low temperature end of their tests; their tests allowed the bentonites to swell as a result of the availability of water at the low temperature end, which then accommodated the shrinkage of the material at the high temperature end of the tests. The elevated temperature tests presented here do not examine the role of the thermal gradient, but are still applicable at the outer edges of the barrier where groundwater will be more readily available, or where high thermal conduction bentonites are used. Here, engineering voids created during the construction of the repository would need to be closed, and the thermal gradient is likely to be small (Zhang et al., 2007, 2009, 2017). In addition, water movement to the outer edges of the clay away from the heat source, as seen in the experiments of Tripathy et al. (2017), will increase the availability of water to facilitate swelling at the outer margins of the barrier. Indeed, results from the FEBEX experiment (Villar et al., 2020) have shown that higher swelling pressures and moisture contents are observed closer to the edge of the barrier after both 5 (Daucausse and Lloret, 2003) and 18 (Villar et al., 2016) years, indicating that saturation

and sealing preferentially occurs around the periphery of the system.

Comparison of the values of the swelling pressure at the end of each test showed that in the elevated temperature case, the final swelling pressures were larger. The swelling pressure data in the elevated temperature tests approached an asymptote in the later stages and showed no indication that the final values would decrease beyond the testing period (Fig. 8). The difference in behaviour between the elevated temperature tests and those presented by Harrington et al. (2020), cannot be attributed to thermal expansion of the pore and interlayer water within the clay structure, expanding due to the increased temperature, because there is little evidence of transient behaviour in the latter stages of the tests associated with water drainage (Fig. 2). Stresses attributed to the expansion of porewater would be expected to dissipate within days as the clay is free to expand, illustrated by the low density of the final sample. This is supported by the cumulative inflow and outflow data (Fig. 4), which exhibited well defined asymptotes indicating minimal water uptake and drainage. However, the stresses may continue to evolve at a slower rate than is suggested by the flow data because of secondary homogenisation of the clay linked to the internal availability of water and small-scale heterogeneities within the original sample (Harrington et al., 2020). In addition, the elevated temperature samples uptook less water over the duration of the test period from the base of the test samples in comparison with the ambient temperature tests of Harrington et al. (2020); this was the case for all three tests (please see Fig. S.14 in the supplementary material). In the 65 mm elevated temperature test (Test 1), the pump recorded a 33.5 mL volume change into the test sample. For the ambient temperature counterpart (Test 1A), the volume of fluid uptake from the base of the sample was 36.5 mL. Accounting for the thermal expansion of 33.5 mL of fluid only gives an increase in volume of 0.485 mL due to the temperature (and therefore an overall volume inflow of 33.99 mL for Test 1). In addition, the rate of uptake of water into the base of the elevated temperature samples was much faster early in the test history (Fig. 4); the elevated temperature cumulative flows reached an asymptote in about 40% of the time required in the ambient temperature tests. This implies that heating the bentonite reduced the test duration by around 60%, and is consistent with the rapid peak and decay of swelling pressures observed in the elevated temperature tests (Figs. 8 and S.15). This significant change in behaviour can be explained by the reduction in viscosity of the test permeant (in this case distilled water) which declines from 1×10^{-3} Pa.s at 20°C to 3.16×10^{-4} Pa.s at 90°C for a pressure of 4500 kPa. This equates to a 68% reduction in viscosity, which is very close to the accelerated hydration time in the elevated temperature tests. Indeed, the experiments by Villar and Lloret (2004) on FEBEX bentonite compacted to 1.58 g/cm^3 showed that hydraulic conductivity increases with increasing temperature up to 80°C, although the increase was slightly lower than the increase with temperature that would have been predicted due to the change in water viscosity alone.

The test apparatus was manufactured from 316-stainless steel, and thus thermal expansion of the test vessel would also have occurred. As the linear thermal expansion coefficient of steel (16×10^{-6} °C^{-1} (Tennent, 1971)) is nearly two orders of magnitude smaller than that of water (2.1×10^{-4} °C^{-1} (Tennent, 1971)), it is unlikely that any expansion of the vessel would have significantly impacted the measured swelling pressures in the elevated temperature tests. Without any expansion of the test vessel at all, the elevated temperature swelling pressures might have been very slightly higher. This is supported in part by the peak swelling pressure measured during Test 4; here the test was conducted in an apparatus constructed from INVAR (Alloy 36) steel, which has a near zero linear thermal expansion coefficient (0.9×10^{-6} °C^{-1} (Tennent, 1971)). In Test 4, the peak axial swelling pressure is slightly above where a linear fit to the peak swelling pressures from Tests 1 and 2 would lie, and the reduced expansion of the test vessel might have contributed to the peak axial swelling pressure being slightly larger (Table 3). It should be noted however, that this test was conducted at 100°C rather than 90°C, as was the case for Tests 1–3, which is likely to also have contributed to this slightly higher peak value. In addition, the peak swelling pressure values would have been more sensitive to the availability and migration of water through the sample than the end-of-test values of swelling pressure, and thus a greater uncertainty on their absolute values exists. It is not thought that the performance of the sensors had any effect on the test results; two different sensor types were used during the testing period (a button load cell with pushrod to translate the stress from the face of the clay, and a membrane-type pressure sensor with direct measurement at the clay surface) and both showed the same trends in the swelling response, and the differences in the absolute values are consistent with differences in the sample dimensions.

Like the swelling pressures, the moisture contents measured in the post-test samples in Tests 1–3 can also be compared with the moisture content data presented by Harrington et al. (2020) for their Tests 1–3 (referred to as Tests 1A-3A here) and with the water content data presented in Dueck et al. (2016). Although their tests were much smaller in both length and duration, with the post-test samples only 25 mm at most and the durations lasting approximately 1 month, the post-test water contents and dry density profiles in Dueck et al. (2016) took the same form as the moisture content and dry density data from this study (Fig. 6). Both sets of data showed much higher moisture contents at the end of the post-test sample that was originally sited next to the void space in the vessel containing the free water. One of the axial swelling tests run by Dueck et al. (2016) (A01–16) included a porewater pressure applied to the sample, and this experiment showed lower final water contents at all positions along the post-test sample. As was observed in the data presented in this paper, sample A01–16 also showed an approximately constant water content for the first half of the sample, before increasing towards the water filled void. Together these tests showed that regardless of the length of the sample, the moisture contents were slow to homogenise. Fig. 6 shows the comparison between the data from this study (Tests 1–3) and the equivalent tests presented in Harrington et al. (2020) (Tests 1A-3A); an individual comparison of the moisture contents for each of the tests can be seen in Fig. S.16 in the supplementary material. The data showed that for a given sample length, the moisture content was uniformly lower in the elevated temperature post-test sample than in the ambient temperature test data; the moisture contents in the zone that would have originally been void space were lower, and there was a shallower gradient between the moisture contents in this zone, and those further down in the sample (closer to the base of the test vessel). Power law fits were used to describe both the moisture content and dry density data from the elevated temperature tests (this study) and the ambient temperature counterparts (Harrington et al., 2020) (Fig. 6), with the dot-dashed lines showing the difference between the power law fit for the equivalent tests in each study. Fig. 6A shows that for longer initial sample lengths, there was less difference between the post-test moisture contents of the pairs of tests with the same sample length. In all tests, the difference in moisture content was most pronounced at the “wetter” end of the sample, where the void would have been at the start of the test. The slightly shallower gradient in the moisture content profiles suggested that the post-test samples from Tests 1–3 (this study) were more homogenised than the Harrington et al. (2020) samples; this was most pronounced for the 75 mm samples (Test 2 and Test 2A), which could be partially attributable to the reversal of the flow direction in the later stages of testing as it is possible that this helped with the redistribution of water within the sample and contributed to the homogenisation (Fig. 6A).

Fig. 6B shows the calculated dry density profile through each sample, based on the moisture content data. The dry densities of the post-test sample material at the base of the test vessel were slightly higher when the test was conducted at elevated temperature. These higher dry densities were consistent with the higher values of swelling pressure recorded at the end of the elevated temperature tests and the lower total volumes of water taken into the sample through the base of the vessel. It is, however, difficult to understand why the elevated temperature post-

test samples exhibited uniformly higher dry densities and lower moisture contents along their length. If the elevated temperature samples were more homogenised, then the clay material within the vessel should have been more evenly distributed along the length of the vessel and the dry densities at the sample base would have been expected to be lower to correspond with higher dry densities at the top of the post-test sample. Moreover, because all of the tests had approximately the same duration, how the moisture contents and dry densities in the sample might evolve over extended periods of time is unclear.

5. Conclusions

Four experiments examining the development of swelling and swelling pressure at an isothermal elevated temperature in bentonite have been conducted. In each experiment, a pre-compacted, sodium-activated MX80 sample was placed at the base of a constant volume pressure vessel next to a water-filled void above the sample, and the sample was able to swell upwards into the void space. Each test used a different starting sample size (ranging between 65 and 95 mm), lasted in excess of 85 days before termination, and was conducted at a temperature of either 90 or 100°C. Throughout the duration of each test, the pore pressure (Tests 1–3) and total stress values (all tests) were recorded, and the tests were terminated once these values had reached an asymptote. All of the tests showed that the bentonite was able to swell to completely fill the void space at an isothermal elevated temperature and under zero hydraulic gradient, creating a small and persistent swelling pressure even at low sample to void ratios.

The pore pressure, and total stress as recorded by the axial and radial load cells, in each experiment evolved in a similar manner, with an early peak in the observed swelling pressures at sensors close to the base of the vessel (next to the starting sample), that decayed towards an asymptote. Sensors located closer to the top of the vessel showed a gradual increase in swelling pressure upwards towards an asymptotic value. By the end of each test, the rates of change within the system were very small, but likely still in a transient phase. The maximum swelling pressure values observed were generally higher for longer starting sample lengths (i.e. higher dry density final samples), and the rate at which the swelling pressure decayed towards an asymptote was different between the tests. The orthogonal stresses measured in Test 4 were largest in the early stages of the test and on the radial sensors closer to the base of the vessel, but became similar for each plane of measurement within ~20–30 days, indicating that the sample was evolving towards radial homogeneity. All test results indicated that the development of pressure was a spatially complex and time consuming process, with only very small changes in pressure occurring during the later stages of each of the tests. This result illustrates that full homogenisation, if it does eventually occur, is an extremely slow process and significantly slower than the timeframe of the tests presented here. Outer sections of the engineered barrier material in a repository are not expected to experience large thermal gradients. However large thermal gradients are expected to occur close to the waste cannisters, thus comparison of the results of this study at isothermal elevated temperature with the case of a strong thermal gradient across the barrier is required. Additional work in this area is therefore needed to examine bentonite behaviour under these conditions.

Tests performed by Harrington et al. (2020) under ambient temperature conditions showed some clear differences in the development of axial and radial swelling pressure in comparison to the elevated temperature tests. Whilst the trends for early peaks in the swelling pressures (measured by sensors located close to the starting sample) that decayed towards an asymptote are similar in both sets of tests, there were some obvious differences in the magnitudes of the stresses and the form of the stress-time curves when compared with the data from this study. Testing at isothermal elevated temperatures showed stresses equilibrated faster than under ambient conditions. This was accompanied by slightly increased homogenisation as evidenced through post-test moisture content measurements and calculated dry densities. This response was accompanied by higher inflow rates during the early stages of testing, caused by the reduction in fluid viscosity. Peak values of axial and radial pressure were lower under thermal loading, though end-of-test values were considerably higher than those observed under ambient conditions. The rates of change observed in the data were very slow in the latter stages of all tests and thus the longevity of these features remains uncertain.

Declaration of Competing Interest

None.

Acknowledgements

This study has been funded by the European Commission (H2020-Euratom-1.2) through the EU-BEACON project (grant agreement ID: 745942) and the HITEC work package of the EU-EURAD project (grant agreement ID: 847593). Clay Technology AB and Svensk Karnbranslehantering AB (SKB) are acknowledged for supplying the MX80 bentonite powder used in this study. The authors thank Dr. Elena Tamayo-Mas of the British Geological Survey for her helpful review of an earlier version of the manuscript, and Dr. Robert Cuss is thanked for his insightful discussion. Simon Holyoake is acknowledged for his assistance with instrumentation of the experimental apparatus and the data acquisition. Humphrey Wallis and Wayne Leman are also thanked for their help in the design and manufacture of the experimental apparatus and the careful preparation of the test samples. This paper is published with the permission of the Director of the British Geological Survey part of United Kingdom Research and Innovation (UKRI).

Appendix A. Supplementary data

Supplementary data to this article can be found online at https://doi.org/10.1016/j.clay.2021.106124.

References

Akesson, M., Börgesson, L., Kristensson, O., 2010. SR-Site Data Report: THM Modelling of Buffer, Backfill and Other System Components. Technical Report, TR-10-44. Svensk Kärnbränslehantering AB (SKB), Stockholm, Sweden.

American Colloid Company, 2001. Industrial Specialties Technical Data, VOLCLAY SPV 200. American Colloid Company, Hoffman Estates, IL, USA.

Andra, 2005. Référentiel des matériaux d'un stockage de déchets à haute activité et à vie longue—Tome 4: Les matériaux à base d'argilites excavées et remaniées. Technical Report, CRPASCM040015B. France.

Bian, X., Cui, Y.J., Li, X.Z., 2018. Voids effect on the swelling behaviour of compacted bentonite. Géotechnique 69 (7), 593–605. https://doi.org/10.1680/jgeot.17.P.283.

Börgesson, L., Hernelind, J., 1999. Coupled Thermo-Hydro-Mechanical Calculations of the Water Saturation Phase of a KBS-3 Deposition Hole: Influence of Hydraulic Rock Properties on the Water Saturation Phase. Technical Report, TR-99-47. Svensk Kärnbränslehantering AB (SKB), Stockholm, Sweden.

Börgesson, L., Johannesson, L.E., Torbjörn, S., Hernelind, J., 1995. Modelling of the Physical Behaviour of Water Saturated Clay Barriers. Laboratory Tests, Material Models and Finite Element Application, Technical Report, TR-95-20. Svensk Kärnbränslehantering AB (SKB), Stockholm, Sweden.

Chapman, N.A., 2006. Geological disposal of radioactive wastes. J. Iber. Geol. 32, 7–14.

Chapman, N., Hooper, A., 2012. The disposal of radioactive wastes underground. Proceed. Geol. Associat. 123, 46–63. https://doi.org/10.1016/j.pgeola.2011.10.001.

Cho, W.J., Lee, J.O., Chun, K.S., 1999. The temperature effects on hydraulic conductivity of compacted bentonite. Appl. Clay Sci. 14, 47–58. https://doi.org/10.1016/S0169-1317(98)00047-7.

Cuisinier, O., Masrouri, F., Pelletier, M., Villieras, F., Mosser-Ruck, R., 2008. Microstructure of a compacted soil submitted to an alkaline PLUME. Appl. Clay Sci. 40 (1-4), 159–170. https://doi.org/10.1016/j.clay.2007.07.005.

Daniels, K.A., Harrington, J.F., Zihms, S.G., Wiseall, A.C., 2017. Bentonite permeability at elevated temperature. Geosciences 7 (3). https://doi.org/10.3390/geosciences7010003.

Daucausse, D., Lloret, A., 2003. Results of "In Situ" Measurements of Water Content and Dry Density. Technical Report, 70-UPC-L-5-012, p. 85. Barcelona, Spain.

Delage, P., Cui, Y.J., Tang, A.M., 2010. Clays in radioactive waste disposal. J. Rock Mech. Geotech. Eng. 2, 111–123. https://doi.org/10.3724/SP.J.1235.2010.00111.

Deniau, I., Devol-Brown, I., Derenne, S., Behar, F., Largeau, C., 2008. Comparison of the bulk geochemical features and thermal reactivity of kerogens from Mol (Boom Clay),

Bure (Callovo-Oxfordian argillite) and Tournemire (Toarcian shales) underground research laboratories. Sci. Total Environ. 389, 475–485. https://doi.org/10.1016/j.scitotenv.2007.09.013.
Dueck, A., Goudarzi, R., Börgesson, L., 2011. Buffer Homogenisation: Status Report. Technical Report, TR-12-02. Svensk Kärnbränslehantering AB (SKB), Stockholm, Sweden.
Dueck, A., Goudarzi, R., Börgesson, L., 2014. Buffer Homogenisation: Status Report 2. Technical Report, TR-14-25. Svensk Kärnbränslehantering AB (SKB), Stockholm, Sweden.
Dueck, A., Goudarzi, R., Börgesson, L., 2016. Buffer Homogenisation: Status Report 3. Technical Report, TR-16-04. Svensk Kärnbränslehantering AB (SKB), Stockholm, Sweden.
Dueck, A., Goudarzi, R., Börgesson, L., 2018. Buffer Homogenisation: Status Report 4. Technical Report, TR-17-04. Svensk Kärnbränslehantering AB (SKB), Stockholm, Sweden.
Dueck, A., Börgesson, L., Kristensson, O., Malmberg, D., Kesson, M., Hernelind, J., 2019. Bentonite Homogenisation: Laboratory Study, Model Development and Modelling of Homogenisation Processes. Technical Report, TR-19-11. Svensk Kärnbränslehantering AB (SKB), Stockholm, Sweden.
Fernández, R., Urs, K., Rodríguez Mäder, M., 2009. Alteration of compacted bentonite by diffusion of highly alkaline solutions. Eur. J. Mineral. 21 (4), 725–735. https://doi.org/10.1127/0935-1221/2009/0021-1947.
Fox, P.J., Stark, T.D., 2015. GCL shear strength and its measurement-ten-year update. Geosynth. Int. 22 (1), 3–47. https://doi.org/10.1680/gein.14.00030.
Fox, P.J., Rowland, M.G., Scheithe, J.R., 1998. Internal shear strength of three geosynthetic clay liners. J. Geotech. Geoenviron. Eng. ASCE 124 (10), 933–944. https://doi.org/10.1061/(ASCE)1090-0241(1998)124:10(933).
Gatabin, C., Talandier, J., Collin, F., Charlier, R., Dieudonne, A.C., 2016. Competing effects of volume change and water uptake on the water retention behaviour of a compacted MX-80 bentonite/sand mixture. Appl. Clay Sci. 121-122, 57–62. https://doi.org/10.1016/j.clay.2015.12.019.
Gens, A., Valleján, B., Sánchez, M., Imbert, C., Villar, M.V., Van Geet, M., 2011. Hydromechanical behaviour of a heterogeneous compacted soil: experimental observations and modelling. Géotechnique 61 (5), 367–386. https://doi.org/10.1680/geot.SIP11.P.015.
Gens, A., Valleján, B., Zandarín, M.T., Sánchez, M., 2013. Homogenization in clay barriers and seals: two case studies. J. Rock Mech. Geotech. Eng. 5, 191–199. https://doi.org/10.1016/j.jrmge.2013.04.003.
Gilbert, R., Fernandez, F., Horsfield, D.W., 1996. Shear strength of reinforced geosynthetic clay liner. J. Geotech. Eng. 122 (4), 259–266. https://doi.org/10.1016/j.sandf.2017.03.007.
Harrington, J.F., Tamayo-Mas, E., 2016. Observational Evidence for the Differential Development of Porewater Pressure within Compact Bentonite and its Impact on Permeability and Swelling Pressure. Technical Report, CR-16-160. British Geological Survey, Nottingham, UK.
Harrington, J.F., Volckaert, G., Noy, D., 2014. Long-term impact of temperature on the hydraulic permeability of bentonite. Geo. Soc. London 400, 589–601. https://doi.org/10.1144/SP400.31.
Harrington, J.F., Daniels, K.A., Tamayo-Mas, E., 2017. Homogenisation on the Laboratory Scale: Development of Porewater Pressure and Stress in Bentonite. Technical Report, CR-17-142. British Geological Survey, Nottingham, UK.
Harrington, J.F., Daniels, K.A., Wiseall, A.C., Sellin, P., 2020. Bentonite homogenisation within engineered cavities: the evolution of swelling pressure during bentonite hydration. Int. J. Rock Mech. Min. Sci. 136 https://doi.org/10.1016/j.ijrmms.2020.104535, 104535.
Herbert, H.J., Kasbohm, J., Sprenger, H., Fernández, A.M., Christian, R., 2008. Swelling pressures of MX-80 bentonite in solutions of different ionic strength. Phys. Chem. Earth 33 (1), S327–S342. https://doi.org/10.1016/j.pce.2008.10.005.
Jia, L.Y., Chen, Y.G., Cui, Y.J., 2019. Effects of a simulated gap on anisotropic swelling pressure of compacted GMZ bentonite. Eng. Geol. 248, 155–163. https://doi.org/10.1016/j.enggeo.2018.11.018.
Johannesson, L.E., Borgesson, L., 1998. Compaction of Bentonite Blocks: Development of Techniques for Production of Blocks with Different Shapes and Sizes. Technical Report, R-99-12. Svensk Kärnbränslehantering AB (SKB), Stockholm, Sweden.
Juvankoski, M., 2010. Description of Basic Design for Buffer (Working Report 2009–131). Technical Report Eurajoki, Finland.
Karnland, O., Pusch, R., Sanden, T., 1994. Buffer Material Characterization. Technical Report, AR-94-60. Svensk Kärnbränslehantering AB (SKB), Stockholm, Sweden.
Karnland, O., Olsson, S., Nilsson, U., 2006. Mineralogy and Sealing Properties of Various Bentonites and Smectite-Rich Clay Materials. Technical Report, TR-06-30. Svensk Kärnbränslehantering AB (SKB), Stockholm, Sweden.
Karnland, O., Olsson, S., Nilsson, U., Sellin, P., 2007. Experimentally determined swelling pressures and geochemical interactions of compacted Wyoming bentonite with highly alkaline solutions. Phys. Chem. Earth 32 (1-7), 275–286. https://doi.org/10.1016/j.pce.2006.01.012.
Komine, H., 2010. Predicting hydraulic conductivity of sand bentonite mixture backfill before and after swelling deformation for underground disposal of radioactive wastes. Eng. Geol. 114, 123–134. https://doi.org/10.1016/j.enggeo.2010.04.009.
Komine, H., Yasuhara, K., Murakami, S., 2009. Swelling characteristics of bentonites in artificial seawater. Can. Geotech. J. 46, 177–189. https://doi.org/10.1139/T08-120.
Lingnau, B.E., Graham, J., Yarechewski, D., Tanaka, N., Gray, M.N., 1996. Effects of temperature on strength and compressibility of sand-bentonite buffer. Eng. Geol. 41, 103–115. https://doi.org/10.1016/0013-7952(95)00028-3.
Martin, P.L., Barcala, J.M., Huertas, F., 2006. Large-scale and long-term coupled thermo-hydro-mechanic experiments with bentonite: the febex mock-up test. J. Iber. Geol. 32 (2), 259–282.
Mokni, N., Barnichon, J.D., Dick, P., Nguyen, T.S., 2016. Effect of technological macro voids on the performance of compacted bentonite/sand seals for deep geological repositories. Int. J. Rock Mech. Min. Sci. 88, 87–97. https://doi.org/10.1016/j.ijrmms.2016.07.011.
Nakayama, S., Sakamoto, Y., Yamaguchi, T., Akai, M., Tanaka, T., Sato, T., Iida, Y., 2004. Dissolution of montmorillonite in compacted bentonite by highly alkaline aqueous solutions and diffusivity of hydroxide ions. Appl. Clay Sci. 27, 53–65. https://doi.org/10.1016/j.clay.2003.12.023.
NDA, 2016. Nuclear Decommissioning Authority Strategy: Effective from April 2016. Technical Report Print ISBN 9781474130431, Web ISBN 9781474130448. https://www.gov.uk/government/publications.
NEA-OECD, 2004. Post-Closure Safety Case for Geological Repositories. Nature and Purpose. Technical Report. Nuclear Energy Agency.
Pusch, R., 1978. Highly Compacted Na Bentonite as Buffer Substance. Technical Report, 74, 1978-02-25. Svensk Kärnbränslehantering AB (SKB), Stockholm, Sweden.
Pusch, R., 1980. Swelling Pressure of Highly Compacted Bentonite. Technical Report, 1980-08-20. Svensk Kärnbränslehantering AB (SKB), Stockholm, Sweden.
Pusch, R., 2002. The Buffer and Backfill Handbook, Part 1: Definitions, Basic Relationships, and Laboratory Methods. Technical Report, TR-02-20. Svensk Kärnbränslehantering AB (SKB), Stockholm, Sweden.
Pusch, R., Karnland, O., Hokmark, H., 1990. GMM - a General Microstructural Model for Qualitative and Quantitative Studies of Smectite Clays. Technical Report, TR-90-43. Svensk Kärnbränslehantering AB (SKB), Stockholm, Sweden.
Romero, E., Gens, A., Lloret, A., 2001. Temperature effects on the hydraulic behaviour of an unsaturated clay. Geotech. Geol. Eng. 19 (3), 311–332. https://doi.org/10.1007/978-94-015-9775-3-5.
Rutqvist, J., 2020. Thermal management associated with geologic disposal of large spentnuclear fuel canisters in tunnels with thermally engineered backfill. Tunn. Undergr. Space Technol. 102, 103454. https://doi.org/10.1016/j.tust.2020.103454.
Rutqvist, J., Borgesson, L., Chijimatsu, M., Nguyen, T.S., Jing, L., Noorishad, J., Tsang, C. F., 2001. Coupled thermo-hydro-mechanical analysis of a heater test in fractured rock and bentonite at Kamaishi Mine - comparison of field results to predictions of four finite element codes. Int. J. Rock Mech. Min. Sci. 38, 129–142. https://doi.org/10.1016/S1365-1609(00)00069-1.
Sellin, P., Leupin, O.X., 2013. The use of clay as an engineered barrier in radioactive waste management—a review. Clay Clay Miner. 61, 477–498. https://doi.org/10.1346/CCMN.2013.0610601.
Sellin, P., Westermark, M., Leupin, O.X., Norris, S., Gens, A., Wiekzorek, K., Tallandier, J., Swahn, J., 2020. Beacon: bentonite mechanical evolution. EPJ Nuclear Sci. Technol. 6, 23. https://doi.org/10.1051/epjn/2019045.
Sibelco Nordic, 2012. Bentonite Volclay MX80. Technical Report. Sibelco Nordic, Goteborg, Sweden.
SKB, 1983. KBS 3 - Final Storage of Spent Nuclear Fuel - KBS-3, III Barriers. Swedish Nuclear Fuel Supply Co/Division KBS (SKBF/KBS). Technical Report, ART-716-3. Svensk Kärnbränslehantering AB (SKB), Stockholm, Sweden.
SKB, 2011. Long-Term Safety for the Final Repository for Spent Nuclear Fuel at Forsmark. Main Report of the SR-Site Project. Technical Report, TR-11-01. Svensk Kärnbränslehantering AB (SKB), Stockholm, Sweden.
Sridharan, A., Rao, A., Sivapullaiah, P., 1986. Swelling pressure of clays. Geotech. Test. J. 9 (1), 24–33. https://doi.org/10.1520/GTJ10608J.
Stark, T.D., Eid, H.T., 1996. Shear behavior of reinforced geosynthetic clay liners. Geosynth. Int. 3 (6), 771–786. https://doi.org/10.1680/gein.3.0084.
Svensson, D., Lundgren, C., Johannesson, L.E., Norrfors, K., 2017. Developing Strategies for Acquisition and Control of Bentonite for a High Level Radioactive Waste Repository. Technical Report, TR-16-14. Svensk Kärnbränslehantering AB (SKB), Stockholm, Sweden.
Svoboda, J., 2013. The experimental study of bentonite swelling into fissures. Clay Miner. 48, 383–389. https://doi.org/10.1180/claymin.2013.048.2.16.
Tang, A.M., Cui, Y.J., 2005. Controlling suction by the vapour equilibrium technique at different temperatures and its application in determining the water retention properties of MX80 clay. Can. Geotech. J. 42 (1), 287–296. https://doi.org/10.1139/t04-082.
Tang, A.M., Cui, Y.J., 2009. Modelling the thermo-mechanical behaviour of compacted expansive clays. Géotechnique 59 (3), 185–195. https://doi.org/10.1680/geot.2009.59.3.185.
Tang, A.M., Cui, Y.J., Barnel, N., 2008. Thermo-mechanical behaviour of a compacted swelling clay. Géotechnique 58 (1), 45–54. https://doi.org/10.1680/geot.2008.58.1.45.
Tennent, R.M., 1971. Science Data Book. Oliver and Boyd. ISBN 0 05 002487 6.
Tripathy, S., Thomas, H.R., Stratos, P., 2017. Response of compacted bentonites to thermal and thermo-hydraulic loadings at high temperatures. Geosciences 7 (53). https://doi.org/10.3390/geosciences7030053.
Villar, M.V., Lloret, A., 2004. Influence of temperature on the hydromechanical behaviour of a compacted bentonite. Appl. Clay Sci. 26, 337–350. https://doi.org/10.1016/j.clay.2003.12.026.
Villar, M.V., Lloret, A., 2008. Influence of dry density and water content on the swelling of a compacted bentonite. Appl. Clay Sci. 39 (1-2), 38–49. https://doi.org/10.1016/j.clay.2007.04.007.
Villar, M.V., Iglesias, R.J., Abós, H., Martínez, V., de la Rosa, C., Manchón, M.A., 2016. FEBEX-DP Onsite Analyses Report. Technical Report, NAB 16-019 NAB 16-012. NAGRA Arbeitsbereicht, Wettingen.
Villar, M.V., Inglesias, R.J., García-Siñeriz, J.L., Lloret, A., Huertas, F., 2020. Physical evolution of a bentonite buffer during 18 years of heating and hydration. Eng. Geol. 264, 105408. https://doi.org/10.1016/j.enggeo.2019.105408.
Wang, Q., Tang, A.M., Cui, Y.J., Delage, P., Barnichon, J.D., Ye, W.M., 2013. The effects of technological voids on the hydro-mechanical behaviour of compacted

bentonite–sand mixture. Soils Found. 53 (2), 232–245. https://doi.org/10.1016/j.sandf.2013.02.004.

Watanabe, Y., Yokoyama, S., 2021. Self-sealing behavior of compacted bentonite–sand mixtures containing technological voids. Geomech. Energy Environ. 25, 100213. https://doi.org/10.1016/j.gete.2020.100213.

Wersin, P., Johnson, L.H., McKinley, I.G., 2007. Performance of the bentonite barrier at temperatures beyond 100: a critical review. Phys. Chem. Earth 32, 780–788. https://doi.org/10.1016/j.pce.2006.02.051.

Ye, W.M., Wan, M., Chen, B., Chen, Y.G., Cui, Y.J., Wang, J., 2013. Temperature effects on the swelling pressure and saturated hydraulic conductivity of the compacted GMZ01 bentonite. Environ. Earth Sci. 68, 281–288. https://doi.org/10.1007/s12665-012-1738-4.

Ye, W.M., Zheng, Z.J., Chen, B., Chen, Y.G., Cui, Y.J., Wang, J., 2014. Effects of pH and temperature on the swelling pressure and hydraulic conductivity of compacted GMZ01 bentonite. Appl. Clay Sci. 101, 192–198. https://doi.org/10.1016/j.clay.2014.08.002.

Zeng, Z., Cui, Y.J., Zhang, F., Conil, N., Talandier, J., 2020. Effect of technological voids on the swelling behaviour of compacted bentonite/claystone mixture. Can. Geotech. J. 57 https://doi.org/10.1139/cgj-2019-0339.

Zhang, C.L., Rothfuchs, T., Jockwer, N., Wieczorek, K., Dittrich, J., Mueller, J., Hartwig, L., Komischke, M., 2007. Thermal Effects on the Opalinus clay. A Joint Heating Experiment of ANDRA and GRS at the Mont Terri URL (HE-D Project). Final Report. Technical Report. Germany.

Zhang, C.L., Wieczorek, K., Rothfuchs, T., Armand, G., Lebon, P., 2009. Responses of the Opalinus clay to heating during the HE-D experiment at Mont Terri. Proceedings of the European Commission TIMODAZ-THERESA International Conference, 29 Sep. – 01 Oct. Technical Report. Luxembourg, pp. 397–401.

Zhang, C.L., Conil, N., Armand, G., 2017. Thermal effects on clay rocks for deep disposal of high-level radioactive waste. J. Rock Mech. Geotech. Eng. 9, 463–478.

Zheng, L., Rutqvist, J., Birkholzer, J.T., Liu, H.H., 2015. On the impact of temperatures up to 200°C in clay repositories with bentonite engineer barrier systems: a study with coupled thermal, hydrological, chemical, and mechanical modelling. Eng. Geol. 197, 278–295. https://doi.org/10.1016/j.enggeo.2015.08.026.